Triazine–Carbosilane Dendrimersomes Enhance Cellular Uptake and Phototoxic Activity of Rose Bengal in Basal Cell Skin Carcinoma Cells

Krzysztof Sztandera, Michal Gorzkiewicz, Mateusz Bątal, Valeria Arkhipova, Nadezhda Knauer, Javier Sánchez-Nieves, Fco Javier de La Mata, Rafael Gómez, Evgeny Apartsin, Barbara Klajnert-Maculewicz

International Journal of Nanomedicine

Dovepress

open access to scientific and medical research

Open Access Full Text Article

ORIGINAL RESEARCH

Triazine–Carbosilane Dendrimersomes Enhance Cellular Uptake and Phototoxic Activity of Rose Bengal in Basal Cell Skin Carcinoma Cells

Krzysztof Sztandera[1], Michał Gorzkiewicz[1,2], Mateusz Bątal[1], Valeria Arkhipova[3,4], Nadezhda Knauer[3,5,6], Javier Sánchez-Nieves[7,8], Fco Javier de la Mata[7–9], Rafael Gómez[7–9], Evgeny Apartsin[3,4,10], Barbara Klajnert-Maculewicz[1]

[1]Department of General Biophysics, Faculty of Biology and Environmental Protection, University of Lodz, Lodz, 90-236, Poland; [2]Department of Molecular Medicine II, Medical Faculty, Heinrich Heine University Düsseldorf, Düsseldorf, 40225, Germany; [3]Institute of Chemical Biology and Fundamental Medicine SB RAS, Novosibirsk, 630090, Russia; [4]Department of Natural Sciences, Novosibirsk State University, Novosibirsk, 630090, Russia; [5]Research Institute of Fundamental and Clinical Immunology, Novosibirsk, 630099, Russia; [6]Clinic for Neurosurgery, Medical Faculty, Heinrich Heine University Düsseldorf, Düsseldorf, 40225, Germany; [7]Departamento de Química Orgánica y Química Inorgánica, UAH-IQAR, Alcalá de Henares, 28805, Spain; [8]Networking Research Center on Bioengineering, Biomaterials and Nanomedicine (CIBER-BBN), Madrid, 28029, Spain; [9]Instituto Ramón y Cajal de Investigación Sanitaria, IRYCIS, Madrid, 28034, Spain; [10]Laboratoire de Chimie de Coordination CNRS, Toulouse, 31077, France

Correspondence: Barbara Klajnert-Maculewicz, Department of General Biophysics, Pomorska 141/143, Łódź, 90-236, Poland, Tel +48 42 635 44 29, Fax +48 42 635 4474, Email barbara.klajnert@biol.uni.lodz.pl

Background: The search for new formulations for photodynamic therapy is intended to improve the outcome of skin cancer treatment using significantly reduced doses of photosensitizer, thereby avoiding side effects. The incorporation of photosensitizers into nanoassemblies is a versatile way to increase the efficiency and specificity of drug delivery into target cells. Herein, we report the loading of rose bengal into vesicle-like constructs of amphiphilic triazine-carbosilane dendrons (dendrimersomes) as well as biophysical and in vitro characterization of this novel nanosystem.

Methods: Using established protocol and analytical and spectroscopy techniques we were able to synthesized dendrons with strictly designed properties. Engaging biophysical methods (hydrodynamic diameter and zeta potential measurements, analysis of spectral properties, transmission electron microscopy) we confirmed assembling of our nanosystem. A set of in vitro techniques was used for determination ROS generation, (ABDA and H_2DCFDA probes), cell viability (MTT assay) and cellular uptake (flow cytometry and confocal microscopy).

Results: Encapsulation of rose bengal inside dendrimersomes enhances cellular uptake, intracellular ROS production and consequently, the phototoxicity of this photosensitizer.

Conclusion: Triazine-carbosilane dendrimersomes show high capacity as drug carriers for anticancer photodynamic therapy.

Keywords: dendrons, amphiphiles, carbosilane, photodynamic therapy, rose bengal, dendrimersomes

Introduction

As the incidence of basal cell carcinoma continues to rise, novel methods of treatment are urgently required.[1] One of the most promising approaches for treating these cancers is photodynamic therapy, which is based on the interplay between molecular oxygen, photosensitizer (PS), and light.[2] This technique is non-invasive and has high efficacy with relatively few side effects. The photodynamic reaction starts with absorption of a light quantum (photon) by the photosensitizer, which then enters an excited singlet state. Because the singlet form is unstable, it is transformed into the triplet state, which triggers a cascade of reactions leading to formation of singlet oxygen and other reactive oxygen species (ROS). This, in turn, leads to uncontrolled oxidation of intracellular structures and ultimately to cell death. Because PS plays a

Received: 3 December 2021
Accepted: 14 February 2022
Published: 15 March 2022

Graphical Abstract

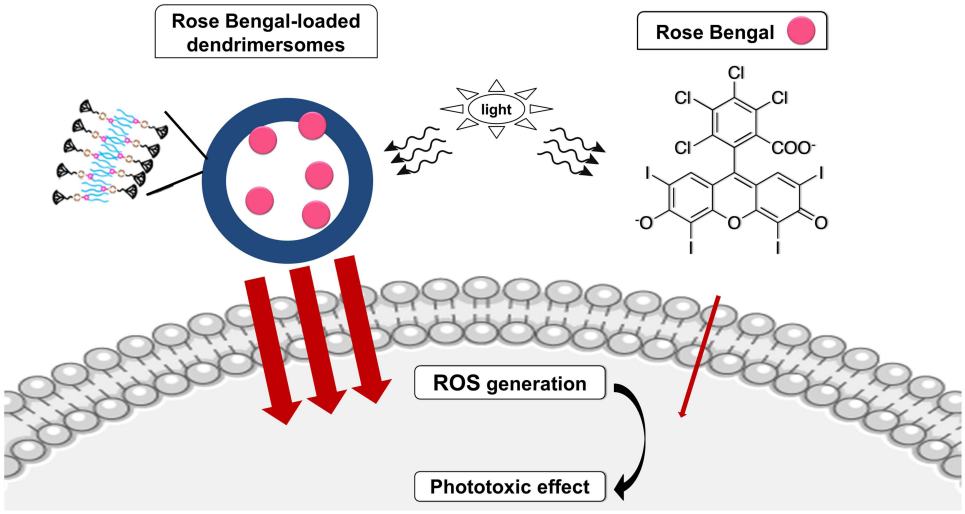

pivotal role in this technique,[3,4] it is important to choose a compound with relevant photodynamic properties, significant half-life, and accumulation inside cancer cells.[5] Rose bengal (RB), an anionic, water-soluble fluorescein derivative that generates singlet oxygen after irradiation with light of 520 nm wavelength, is one of the most extensively tested photosensitizers and holds great promise for medical applications.[6,7] However, the anionic nature of RB limits its use in PDT due to low cellular uptake,[8] necessitating the use of appropriate drug delivery systems. Modern nanotechnology methods can overcome this obstacle, yielding nanoparticles with strictly defined properties that can act as carriers for drugs in various therapies, including PDT.[4,9] A number of PS nanocarriers has been reported so far,[10] including liposomes,[11] dendrimers[12–15] and polymersomes[16] as well as dendrimersomes.[17–19]

Dendrimersomes are three-dimensional structures built of self-assembling amphiphilic dendrons.[20] The final properties of dendrimersomes are dependent on the number of hydrophilic branches, which decide about dendrimersomes generation, the distribution of chemical groups inside or outside the branches, as well as appropriately selected pH-responsive or hydrophobic elements. Optimized synthesis of dendrons from carefully adjusted elements results in properties that enable the formation of a bilayers, similar to the liposomes, wherein drugs can be loaded.[21,22] The present work focus on triazine–carbosilane dendrimersomes of the second (G2) and third (G3) generation. These compounds have a branched hydrophobic part, a triazine cycle (the protonation of which, depending on the pH of the environment, allows the structure of the dendrimersome to loosen or shorten), a piperazine ring (which plays the role of the linker), and the hydrophilic part. The obtained dendrimersomes have a compact (closed) structure in a neutral pH, opening in an acidic environment.[20] This allows for a selective delivery and release of the cargo only in the tumor environment.[23] In this study, we report the assembly of triazine–carbosilane dendron-based dendrimersomes loaded with rose bengal, as well as proof-of-concept studies of their efficacy in PDT.

Materials and Methods

Materials

RB, fetal bovine serum (FBS), penicillin/streptomycin solution, trypsin-EDTA solution, ABDA probe [9,10-antherachenediyl-bis(methylene) dimalonic acid], MTT [3-(4,5-dimethyl-2-thiazolyl)-2,5-diphenyl-2H-tetrazolium bromide], and HEPES (4-(2-hydroxyethyl)-1-piperazineethanesulfonic acid) were purchased from Sigma-Aldrich (Taufkirchen, Germany). Dulbecco's phosphate buffered saline without calcium and magnesium (DPBS) was purchased from Biowest (Nuaillé, France). HBSS (Hanks' Balanced Salt Solution) and 154 CF culture medium were obtained from

Gibco/ThermoFisher Scientific (Waltham, MA, USA). Chelex 100 Resin was obtained from Bio-Rad (Hercules, CA, USA). H_2DCFDA (2′,7′ dichlorodihydrofluorescein diacetate) was purchased from Invitrogen/ThermoFisher Scientific (Waltham, MA, USA). Dimethyl sulfoxide (DMSO) was purchased from POCH (Gliwice, Poland). Murine basal cell carcinoma lines (AsZ, BsZ, CsZ) were provided by Dr. Ervin Epstein (Children's Oakland Research Institute, Oakland, CA, USA).

Organic solvents were dried and freshly distilled under argon prior to use. Chemicals were obtained from commercial sources and used as received. Water solutions of chemicals, amphiphiles and buffer solutions were prepared using milliQ® deionized water. Sonication of amphiphile solutions was done in a Sonorex Super RK 31 H ultrasonic bath (Bandelin Electronic, Berlin, Germany).

Methods

Analytical and Spectroscopic Techniques

^{1}H and ^{13}C spectra were recorded on Varian Unity VXR-300 (Varian Inc., Palo Alto, CA) and Bruker AV400 (Bruker, Karlsruhe, Germany) instruments. Chemical shifts (δ, ppm) were measured relative to residual ^{1}H and ^{13}C resonances for $CDCl_3$ used as solvent. ESI-TOF analysis was carried out in an Agilent 6210 TOF LC/MS mass spectrometer (Agilent, Santa Clara, CA). UV-vis absorbance spectra were acquired using a Jasco V-650 spectrophotometer (Jasco, Cremella, Italy). Fluorescence emission spectra were obtained on an LS 55 fluorescence spectrometer (PerkinElmer, Waltham, MA, USA) at 25°C.

Synthesis of Dendritic Amphiphiles

Vinyl-terminated dendron precursors G2, G3 bearing bromine in the focal point were obtained as described elsewhere.[24] 2,4-dodecylamino-6-chloro-1,3,5-triazine, 2,4-dodecylamino-6-piperazino-1,3,5-triazine, vinyl-terminated dendron G2 and amphiphilic dendron G2 were synthesized as previously described.[20] Only the synthesis of new compounds is described herein.

Vinyl-Terminated Dendron G3

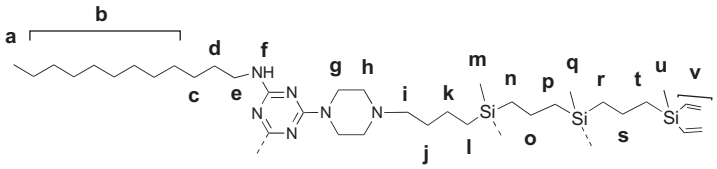

2,4-didodecylamino-6-piperazino-1,3,5-triazine (350 mg, 0.66 mmol), vinyl-terminated carbosilane dendron BrG_3V_8 (544 mg, 0.6 mmol), K_2CO_3 (124 mg, 0.9 mmol) were mixed in 30 mL acetone in a sealed ampule with catalytic amounts of 18-crown-6 and KI added. The reaction mixture was stirred for 24 h at 90 °C. The reaction completion was monitored by TOCSY ^{1}H NMR following the disappearance of $BrCH_2$ protons. When the reaction was over, the solvent was removed under vacuum, the residue was dissolved in ethyl acetate and washed with brine. The organic phase was dried over Na_2SO_4, and the solvent was removed. The crude product was purified by silica gel column chromatography (eluent: ethyl acetate:hexane 1:1) to yield functionalized dendron as light-yellow oil (590 mg, 72%).

^{1}H NMR (400 MHz, $CDCl_3$) δ −0.11 (s, 6H, H_q), −0.10 (s, 3H, H_m), 0.11 (s, 12H, H_u), 0.45 (m, 2H, H_l), 0.51 (m, 6H H_n, H_p, H_r), 0.69 (m, 8H, H_t), 0.86 (t, J = 6.7 Hz, 6H, H_a), 1.21–1.38 (m, 50H, H_b, H_c, H_k, H_o, H_s), 1.51 (t, J = 7.3 Hz, 6H, H_d, H_j), 2.34 (t, J = 7.9 Hz, 2H, H_i), 2.43 (m, 4H, H_h), 3.31 (m, 4H, H_g), 3.77 (s, 4H, H_e), 4.81 (s, 2H, H_f), 5.63–6.19 (m, 24H, H_v). ^{13}C NMR (101 MHz, $CDCl_3$) δ −5.2, −5.1, −5.0, 13.9, 14.1, 18.3, 18.5, 18.7 (m), 18.9, 22.1, 22.7, 26.9, 29.1–29.9 (m), 30.7, 30.9, 31.9, 40.7, 42.9, 53.2, 58.7, 132.6, 137.2, 164.7, 166.1. MS: $[M+H]^+$ 1357.03 amu (calcd 1357.67 amu).

Amphiphilic Dendron G3

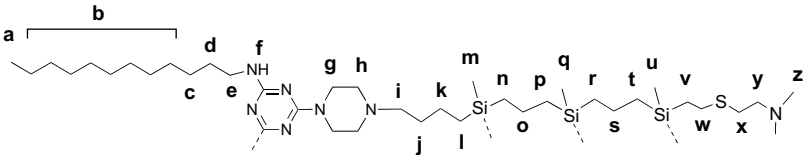

Functionalized vinyl-terminated dendron (400 mg, 0.3 mmol), 2-(dimethylamino) ethanethiol hydrochloride (340 mg, 2.4 mmol) and dimethoxyphenylacetophenone (DMPA) (16 mg, 0.06 mmol) were dissolved in 5 mL of mixture THF: CH_3OH (1:2). The reaction mixture was deoxygenated by bubbling argon and irradiated by UV for 2 h (365 nm, 120W). Then, another 16 mg (0.06 mmol) of DMPA was added, and the reaction mixture was irradiated for another 2 h. The reaction completion was monitored by ^{1}H NMR. After the reaction was completed, the solvents were removed under vacuum and then the residue was dissolved in methanol. Afterward, it was precipitated in diethyl ether, and after the solvent was separated, the solid was dried under vacuum to afford the desired dendron as light-yellow solid (500 mg, 68%). For characterization, the dendron was deprotonated with K_2CO_3.

^{1}H NMR (400 MHz, $CDCl_3$) δ −0.11 (m, 9H, H_m, H_q), −0.02 (s, 6H, H_u), 0.50 (m, 16H, H_l, H_n, H_p, H_r), 0.58 (m, 8H, H_t), 0.86 (s, 22H, H_a, H_v), 1.18–1.33 (m, 50H, H_b, H_c, H_k, H_o, H_s), 1.49 (m, 6H, H_d, H_j), 2.23 (s, 24H, H_z), 2.32 (m, 2H, H_i), 2.39 (m, 4H, H_h), 2.46 (m, 16H, H_y), 2.53 (m, 16H, H_w), 2.60 (m, 16H, H_x), 3.30 (s, 4H, H_g), 3.73 (s, 4H, H_e), 4.70 (s, 2H, H_f). ^{13}C NMR (101 MHz, $CDCl_3$) δ −5.3, −5.1, −5.0, 14.0, 14.1, 14.6, 18.3, 18.4, 18.7, 22.1, 22.6, 27.0, 27.8, 29.3–30.0 (m), 30.9, 31.9, 37.0, 40.6, 42.9, 45.4, 53.3, 59.3, 127.7, 128.5, 165.0, 166.2.

Preparation of Rose Bengal-Loaded Dendrimersomes

Solutions of rose bengal (5 μL, 10 mM) and dendron (G2 or G3, 10 μL, 10 mM) were quickly mixed in 1 mL of deionized water (mQ). The mixture was sonicated for 30 min and then incubated for 48 h at room temperature (RT). Empty dendrimersomes were prepared analogously. A UV-vis spectrum of the mixture was recorded (before dialysis). In the next step dendrimersomes loaded with RB (G2-RB and G3-RB) were purified by dialysis in SnakeSkin™ Dialysis Tubing (3.5K MWCO, 22 mm, ThermoFisher, Waltham, Massachusetts, USA) against deionized water (mQ) for 6 h, changing water three times during this time. A UV-vis spectrum of the mixture was recorded (after dialysis). The percentage of encapsulated drug (encapsulation efficency) was estimated from the ratio of absorbance values at 565 nm (before and after dialysis).

Hydrodynamic Diameter

The water solution of RB-loaded dendrimersomes (G2-RB or G3-RB, 400 μL) was mixed with 20 μL phosphate buffer (200 mM, pH 7) and incubated in RT for 2 h. The solutions were subsequently placed in the low volume sizing cuvettes (ZEN0112, Malvern). Measurements of hydrodynamic diameter were performed with the use Dynamic Light Scattering (DLS) on Zetasizer Nano ZS (Malvern Instruments Ltd., Malvern, UK) at 25°C. The data were analyzed using the Malvern software.

Zeta Potential

For zeta potential measurements, 50 μL of G2-RB or G3-RB was added to 1 mL of deionized water (mQ). Then the solutions were places in the folded capillary cells (DTS 1070, Malvern) and the zeta potential was measured with the use of Zetasizer Nano ZS (Malvern Instruments Ltd., Malvern, UK) at 25°C. The data were analyzed using the Malvern software.

Transmission Electron Microscopy

Transmission electron microscopy (TEM) images were obtained using a Veleta digital camera (EM SIS, Muenster, Germany) mounted on a JEM 1400 transmission electron microscope (JEOL, Japan) at the accelerating voltage of 80 kV. Samples were stained with 0.1% uranyl acetate.

Spectroscopy Studies

Absorbance Measurement All measurements were performed in mQ water at RT on a Jasco V-650 spectrophotometer. Spectra were recorded in a wavelength range from 300 to 650 nm. Optical path length was 1 cm. The measurements were carried out for tested compounds at 5 μM concentration of RB. Deionized water (mQ) was used as a reference for all measurements.

Fluorescence Measurement All samples were prepared in mQ water and measured in quartz cuvettes on LS 55 fluorescence spectrophotometer (PerkinElmer, Waltham, MA, USA). The excitation wavelength was set to 525 nm, and spectra were recorded between 540 and 650 nm. Excitation and emission slits were 5 and 7.5 nm, respectively. The measurements were carried out for tested compounds at 1 μM concentration of RB.

Release Studies

To evaluate the rate of RB release from the dendrimersomes, 1 mL solution of G2-RB or G3-RB (50 μM of RB) dissolved in distilled water was enclosed in a dialysis membrane tube (SnakeSkin™ Dialysis Tubing, 3.5K MWCO, 22 mm, ThermoFisher, Waltham, Massachusetts, USA) and dialyzed against phosphate buffer (pH 5.5) at RT, changing buffer after each two hours of dialysis. Aliquots from the internal phase were collected after 0, 0.25, 0.5, 1, 2, 4, 6 and 24 h, and the RB absorbance was analyzed similarly to spectroscopy studies. The percentage of release was determined regarding the first sample (0 h, 100% of initial absorbance). The experiment was performed in triplicates.

Singlet Oxygen Generation

The singlet oxygen generation assay was performed with use of ABDA probe. The solution of free photosensitizer (RB), G2 and G3 empty dendrimersomes, G2-RB and G3-RB were prepared in DPBS at 0.25, 0.5, 1, 2 μM final concentration of RB. Then 100 μL of each solution was transferred to the 96-well black plate. All measurements were recorded using fluorescence microplate reader (Fluoroskan Ascent FL, ThermoFisher, Waltham, MA, USA). The excitation and emission wavelength were set to 355 and 430 nm, respectively. First measurement was recorded without probe in order to verify whether compounds under study exhibit fluorescence in this range. Then, 20 μL of 30 μM ABDA was added to each sample and the fluorescence intensity of samples with ABDA was measured. Subsequently, the plate was irradiated for 5 min with the lamp equipped with a filter emitting visible light in the range of 385−780 nm and the light dose of 2.4 J/cm^2 per minute (Q. Light Pro Unit, Q. Products AG, Switzerland). Fluorescence intenstiy of probe was measured after each 5 minutes of irradiation up to 1 h. Then, the slopes of the fluorescence intensity curves were considered for the measurement of singlet oxygen generation, and the results were presented as percentage of singlet oxygen generation in control (DPBS irradiated with probe).

Cell Cultures

Murine basal cell carcinoma lines (AsZ, BsZ and CsZ) were cultured in 154-CF medium with 5% penicillin/streptomycin, 0.05 mM calcium, and 2% chelexed, heat-inactivated fetal bovine serum (FBS). Cells were cultured in T-75 culture flasks at 37 °C, 5% CO_2 and subcultured every 2 or 3 days. The number of viable cells was determined by trypan blue exclusion assay with the use of Countess Automated Cell Counter (Invitrogen, Carlsbad, California, USA). For harvesting the cells, 0.25% (w/v) trypsin−0.03% (w/v) EDTA solution was used.

ROS Generation Assay

AsZ, BsZ, CsZ cells were seeded into 96-well plates at a density of 1×10^4 cells per well. After 24 h of incubation (37 °C, 5% CO_2), 100 μL of free photosensitizer (RB), G2 or G3 empty dendrimersomes, G2-RB or G3-RB dissolved in fresh culture medium was added to the cells at final RB concentrations of 0.25, 0.5, 1, 2 μM. Cells were incubated with tested compounds for 5 h (37 °C, 5% CO_2). Then the medium was replaced with 100 μL fresh Hank's Balanced Salt Solution (HBSS). The 20 μL of H_2DCFDA solution (final concentration: 2 μM) was added to each sample and cells were incubated for 20 min in dark (37 °C, 5% CO_2). Cells were subsequently washed with 100 μL of HBSS and fluorescence intensity of non-irradiated cells was measured using fluorescence microplate reader PowerWave HT Microplate Spectrophotometer (BioTek, USA). Then the cells were irradiated for 30 min (2.4 J/cm^2 per minute) with use of Q. Light Pro Unit lamp and the fluorescence intensity of DCF was measured. The ROS level was calculated as DCF

fluorescence intensity increase and presented as a percentage of ROS production in control samples (without tested compounds). Every measurement was corrected by subtraction of the background fluorescence intensity.

Cellular Uptake

AsZ, BsZ, CsZ cells were seeded into 24-well plates at a density of 1×10^5 cells per well and incubated for 24 h (37 °C, 5% CO_2). Next, 300 µL of free photosensitizer (RB), G2-RB or G3-RB was added to the cells in fresh culture medium at the final RB concentration of 5 µM. The cells were incubated with compounds up to 4 h. Following the incubation, the compounds were discarded, and cells were washed with DPBS. Next, the cells were detached from the plates using trypsin-EDTA solution. Then the fresh culture medium was added to the cells, the samples were gently mixed and collected for measurements. For estimation of the cellular uptake, the fluorescence of the samples was measured using flow cytometry (LSRII, Becton Dickinson). The excitation and the emission filters were 520 and 570 nm, respectively.

Confocal Microscopy

AsZ, BsZ, CsZ cells were seeded into 96-well black plate with transparent glass bottom at a density of 1×10^4 cells per well. After 24 h of incubation in standard conditions, medium was replaced with 100 µL of free photosensitizer (RB), G2-RB or G3-RB dissolved in fresh culture medium at the final RB concentration of 5 µM. The plates were incubated for 4 h in the dark (37 °C, 5% CO_2). Cells were subsequently washed with PBS and fixed with 4% formaldehyde solution for 15 min. Then the solution of Phalloidin–Atto 633 (1:400) was added to each well for 20 minutes to stain F-actin in cell membrane. The cells were washed with DPBS and the solution of 5 µM Hoechst 33342 was added to the cells for additional 15 min to stain DNA in cell nucleus. Following the incubation, cells were washed with DPBS and submerged in 100 µL of fresh DPBS. The images were taken with Leica TCS SP8 confocal microscope.

Cytotoxicity Studies

AsZ, BsZ, CsZ cells were seeded into 96-well plates at a density of 2.5×10^4 cells per well. After 24 h of incubation (37° C, 5% CO_2) 100 µL of free photosensitizer (RB), G2 or G3 empty dendrimersomes, G2-RB or G3-RB dissolved in fresh culture medium were added to the cells at 0.25, 0.5, 1, 2 µM final concentrations of RB. Cells were incubated with tested compounds for 5 h (37 °C, 5% CO_2). Then the medium was replaced with DPBS buffer and cells were irradiated for 30 min (2.4 J/cm^2 per minute) with Q. Light Pro Unit lamp. Immediately after irradiation, DPBS was replaced with fresh culture medium, and cells were incubated for 24 h as post-PDT incubation. Additionally, the "dark" toxicity (without irradiation) was evaluated. The cell viability was measured using MTT assay. MTT was added to the wells at a final concentration of 0.5 mg/mL and the plates were incubated for 2 h (37 °C, 5% CO_2). After incubation, formazan crystals were dissolved in DMSO, and the absorbance was read at 570 nm using the PowerWave HT Microplate Spectrophotometer (BioTek, USA).

Statistical Analysis

Mann–Whitney test was used for testing statistical significance in release studies. For the rest of the experiments, two-way ANOVA for concentration series and compounds followed by post-hoc Tukey's test for pairwise difference testing were used. In all tests, p-values < 0.05 were considered statistically significant. Data were collected from at least three independent experiments and presented as arithmetic mean ±SD.

Results

Amphiphilic triazine–carbosilane dendrons (Figures 1 and 2) were synthesized in a convergent way by a conjugation of hydrophobic triazine block and vinyl-terminated dendrons G2 and G3 by a piperazine linker followed by the functionalization of dendron periphery with cationic groups via a thiol-ene reaction. Amphiphilic dendron G2 was reported recently,[20] the dendron G3 has been obtained herein for the first time. Features of the architecture, such as combination of hydrophobic and hydrophilic fragments in the structure, allow for the self-association of dendrons into supramolecular constructions – dendrimersomes.

Dendrimersomes formed at neutral pH have mean diameter of 40–50 nm and in the acidic conditions they reorganize into larger particles (100–150 nm diameter) (Figure 3).

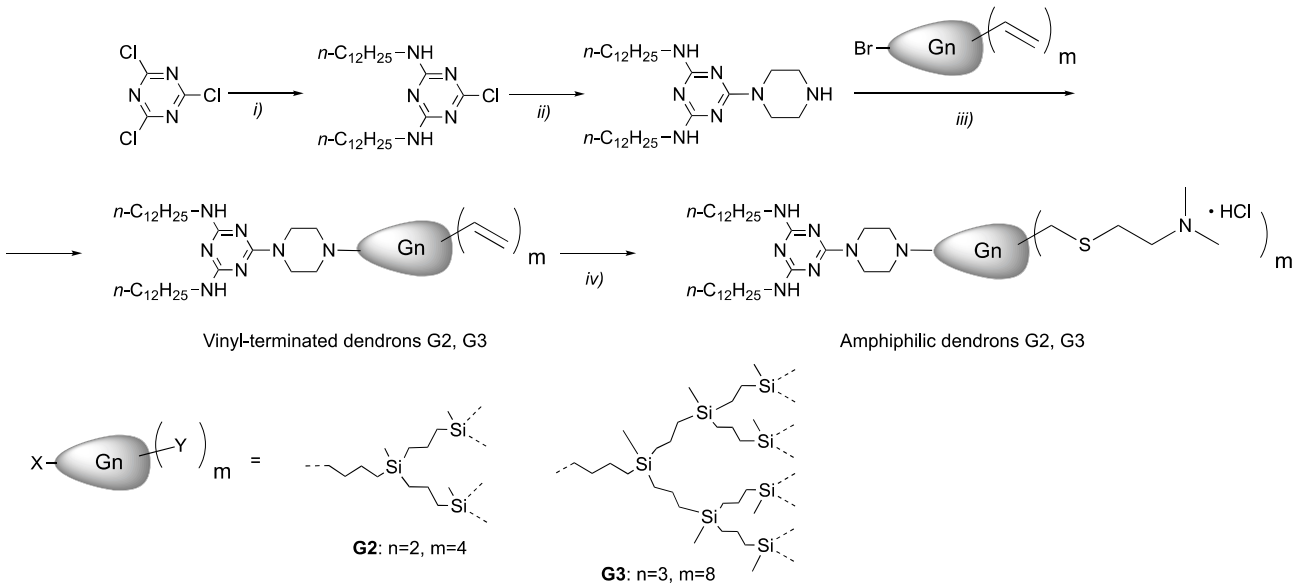

Figure 1 Synthesis of the amphiphilic dendron: *(i)* n-$C_{12}H_{25}NH_2$, $CHCl_3$, NaOH (aq.); *(ii)* piperazine, $CHCl_3$; *(iii)* BrG_nV_m, K_2CO_3, 18-crown-6, KI, acetone; *(iv)* $HS(CH_2)_2N(CH_3)_2$·HCl, DMPA, 365 nm UV, THF:CH_3OH.

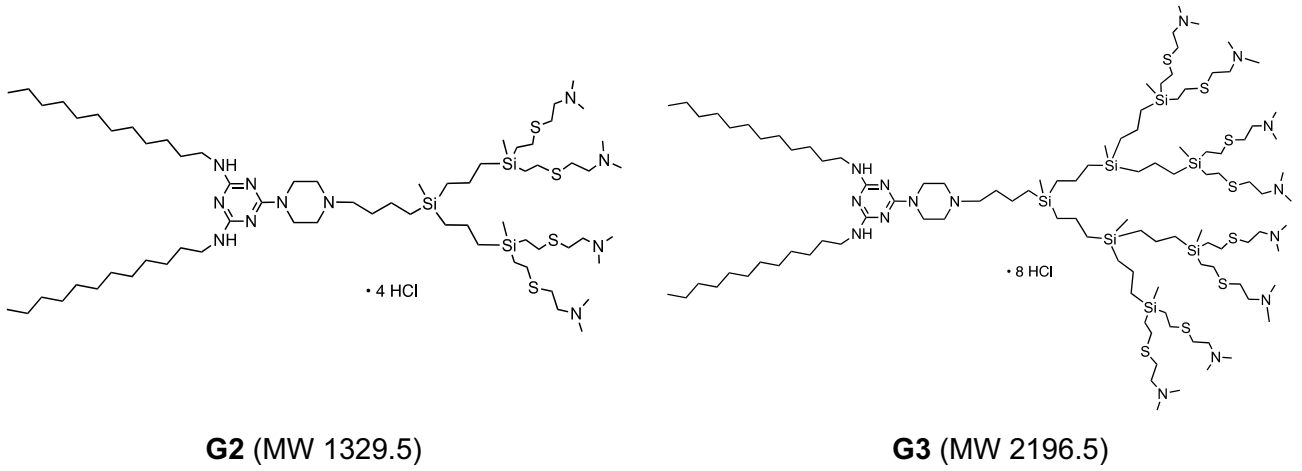

Figure 2 Structures of amphiphilic triazine–carbosilane dendrons of 2nd and 3rd generation.

The zeta potential as well as hydrodynamic diameter of evaluated compounds is similar, regardless generation of dendrimersomes (Table 1).

Both absorbance and fluorescence emission spectra of RB-loaded dendrimersomes showed a red shift of the maximum and a decrease in the intensity compared with free RB. After purification by dialysis, absorbance (Figure 4) and fluorescence intensities (Figure 4 inset) were further decreased. Based on changes in absorbance, the estimated percentage of RB encapsulation was 76% for G2 and 89% for G3.

Because the structures of both G2 and G3 dendrimersomes were compact ("closed") at neutral pH and more loose ("open") in slightly acidic pH (Figure 3), we monitored release of RB from the dendrimersomes at pH 5.5.[20] The RB release rate differed significantly between the two generations of dendrimersomes (G2-RB and G3-RB). RB release from G3-RB was much slower during dialysis, although the release of RB from the two types of dendrimersomes was similar after 24 h of dialysis (Figure 5). Generation of singlet oxygen by RB and G2-RB at the highest concentration of PS was approx. 3-fold higher than in the control, with no significant differences between the two compounds. We observed a

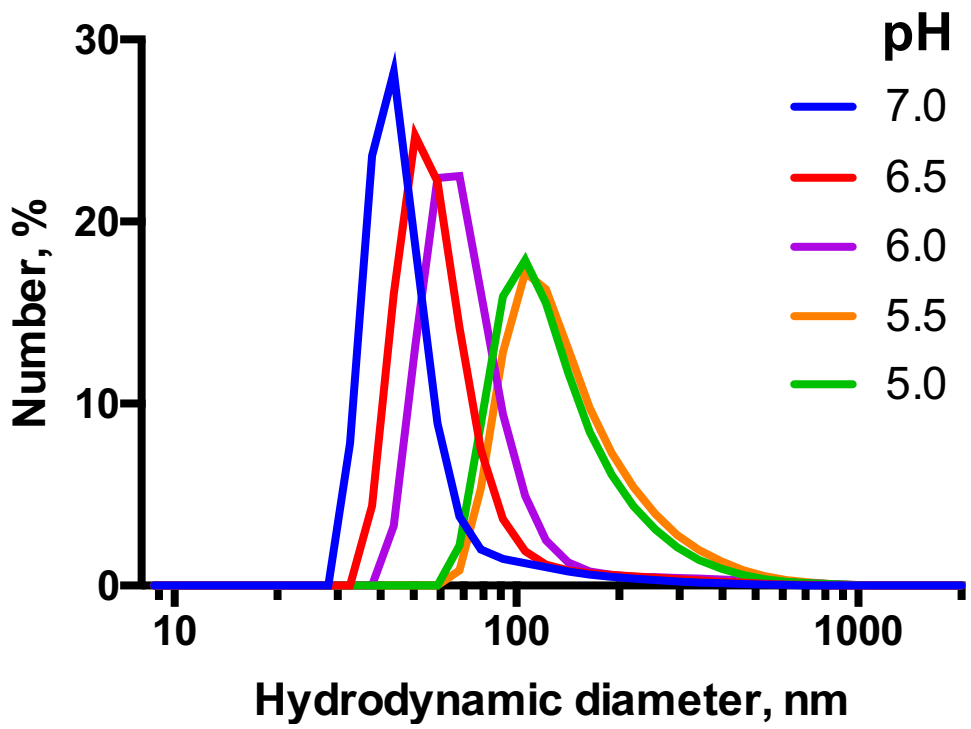

Figure 3 DLS profiles for supramolecular associates of the amphiphilic dendron G3 (100 μM) exposed to different pH in 10 mM Na-phosphate buffer.

statistically significant difference between free RB and G3-RB; in the case of the latter, the level of singlet oxygen was 5-fold higher than in the unstimulated control (Figure 6).

Cellular uptake of G2-RB and G3-RB was significantly higher in comparison to free RB. In all cell lines almost 80% of tested cells absorbed RB encapsulated in dendrimersomes. Moreover, the percentage of RB-positive cells reached a plateau after 0.5 h from the start of the experiment (Figure 7A and Figure S1). Consistent with the results of flow cytometry experiments, confocal micrographs of the AsZ (Figure 7B), BsZ (Figure S2), and CsZ (Figure S3) cell lines revealed that both G2-RB and G3-RB were taken up to a greater extent than free RB.

Encapsulation of RB in both dendrimersomes caused a significant increase in ROS production in all cell lines to a similar degree. Figure 8A shows representative results from AsZ cell lines, and ROS production in BsZ and CsZ cell lines is shown in Figure S4. At RB concentrations of 1 and 2 μM, we observed statistically significant differences between free RB and G2-RB or G3-RB. At the highest concentration, fluorescence intensity of the probe increased 10-fold for both RB-loaded dendrimersomes relative to the untreated control. The phototoxic effect was observed in all cell lines under study (AsZ, BsZ, and CsZ) (Figures 8B and S5). Both RB-loaded dendrimersomes (G2-RB and G3-RB) exerted significantly higher cytotoxic effects after irradiation, and this trend was maintained in all cell lines. At the

Table 1 Size and Zeta Potential of Rose Bengal-Loaded Dendrimersomes (G2-RB and G3-RB) as Well as Free Dendrimersomes (G2 and G3).

	G2-RB	G3-RB	G2	G3
PDI	0.38 ± 0.14	0.31 ± 0.10	0.27 ± 0.007	0.31 ± 0.012
Hydrodynamic diameter [nm]	55.47 ± 23.97	72.64 ± 36.49	36.68 ± 7.933	55.75 ± 9.696
Zeta potential [mV]	39.17± 3.17	39.50 ± 3.59	37.25 ± 2.60	44.24 ± 2.26
Drug loading capacity [%]	>22.5	>17.6		

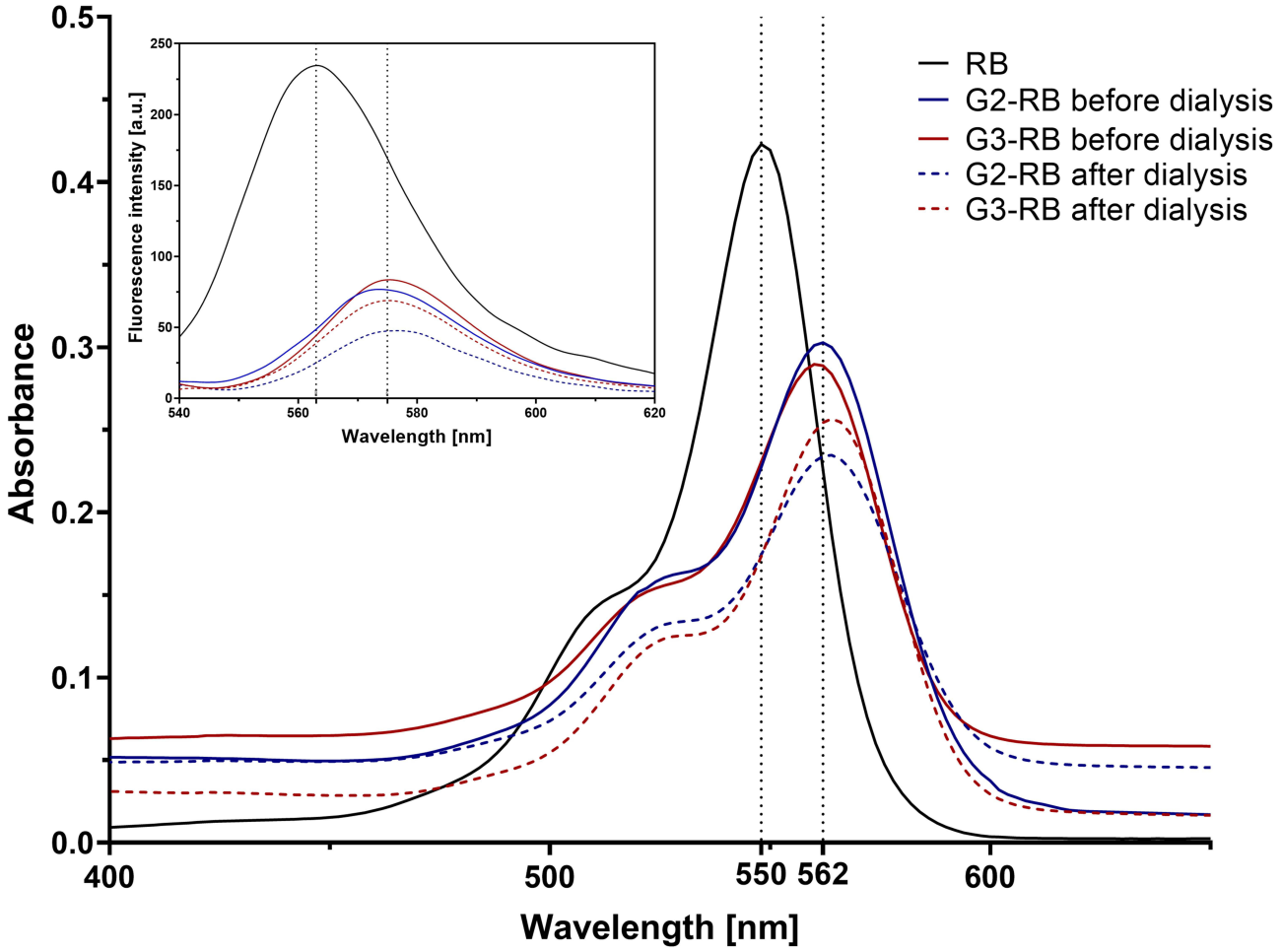

Figure 4 Changes in fluorescence and absorbance spectra of RB after encapsulation within dendrimersomes. The measurements of absorbance and fluorescence intensity were carried out for the tested compounds at RB concentrations of 5 and 1 μM, respectively.

highest concentration, the viability of cells decreased to approx. 25%, whereas free RB decreased cell viability only to approx. 75%. IC_{50} values are presented in Table S1. We also observed a lack of dark toxicity of the tested compounds in all cell lines (Figure S6). Moreover, empty dendrimersomes exerted neither phototoxicity nor dark toxicity (Figure S7).

Discussion

Basal cell carcinoma is the most frequently diagnosed type of skin cancer in humans, but accurate estimation of the number of cases is difficult due to the fact that only a small fraction of the cancers is correctly diagnosed. However, we do know that over a lifetime, the likelihood of developing this type of cancer is as high as 30%, irrespective of genetic aspects and environmental factors. Currently, basal cell carcinoma is treated using several conventional techniques: surgery, chemotherapy, and radiotherapy; however, all of these approaches are associated with numerous side effects.[1,25] Accordingly, highly efficient novel treatment methods are urgently required.

Photodynamic therapy (PDT) is a noninvasive alternative to the aforementioned techniques. PDT exploits three inseparable elements (photosensitizer, oxygen, and light) that act together and start a cascade of reactions generating singlet oxygen (II type of PDT reactions) and/or reactive oxygen species, and the oxidation of intracellular structures such as fatty acids, nucleic acids, and proteins (type I PDT reactions).[4] Rose bengal (RB) deserves special attention because it generates singlet oxygen with higher efficiency than other photosensitizers.[26,27] However, free RB has a tendency to aggregate in aqueous solutions and is characterized by limited cell membrane penetration.[8] Hence, the search for an appropriate carrier for RB is still ongoing. A promising way to increase bioavailability of RB is to deliver it in

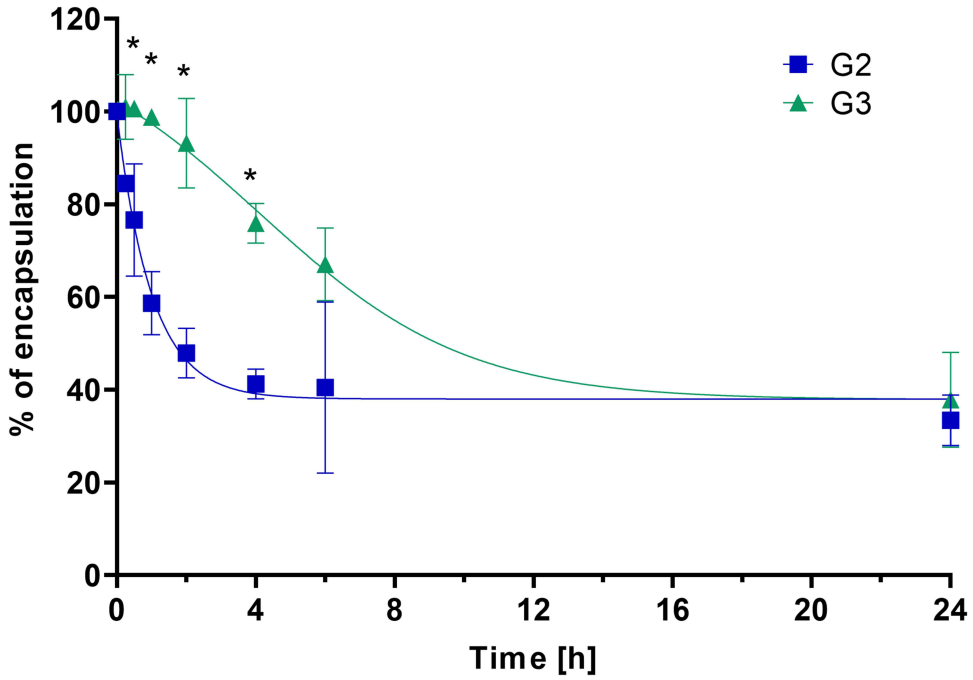

Figure 5 Release of RB from G2-RB and G3-RB dendrimersomes at pH 5.5. Percentage of release was determined relative to the first sample (0 h, 100% of initial absorbance). *Statistically significant difference at $p < 0.05$ between the two generations of dendrimersomes. Data are presented as means ± SD, n=3.

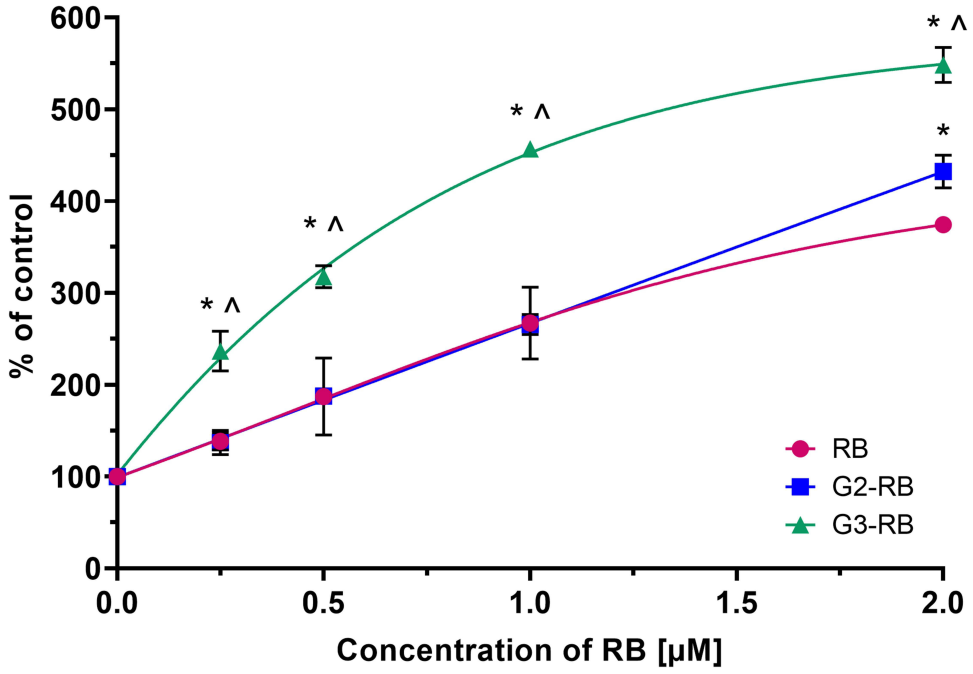

Figure 6 Singlet oxygen generation by free RB and dendrimersomes loaded with RB (G2-RB and G3-RB), determined using an ABDA probe. *Statistically significant difference at $p<0.05$ between G3-RB or G2-RB and RB. ^ Statistically significant difference at $p<0.05$ between G2-RB and G3-RB. Data are presented as means ± SD, n=3.

nanoformulations.[8] To date, various types of RB-loaded nanocarriers have been designed for skin cancer PDT in vitro and in vivo, including lipid-based formulations[28–30] polymeric nanoparticles,[31–33] upconversion nanoparticles,[34,35] inorganic nanoparticles[36] and so on.

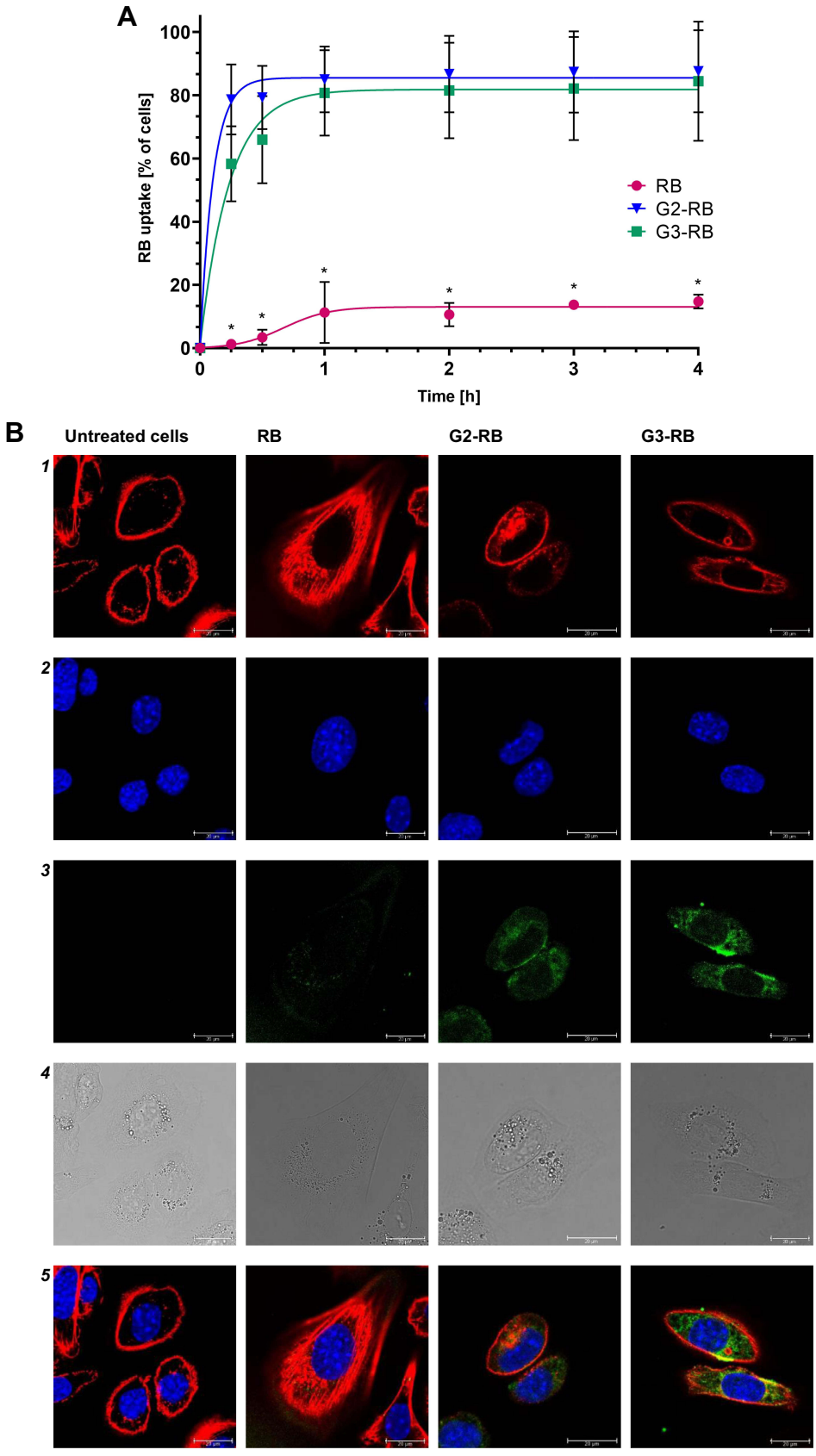

Figure 7 (**A**) Uptake of free RB and dendrimersomes loaded with RB (G2-RB and G3-RB) by AsZ cells. Data are presented as means ± SD, n=3. *Statistically significant difference at $p<0.05$ between evaluated compounds and RB. (**B**) Confocal micrographs: (1) Phalloidin–Atto 633; (2) Hoechst 33342; (3) rose bengal; (4) bright field image; (5) merge of channels 1, 2, and 3. Scale bar represents 20 µm.

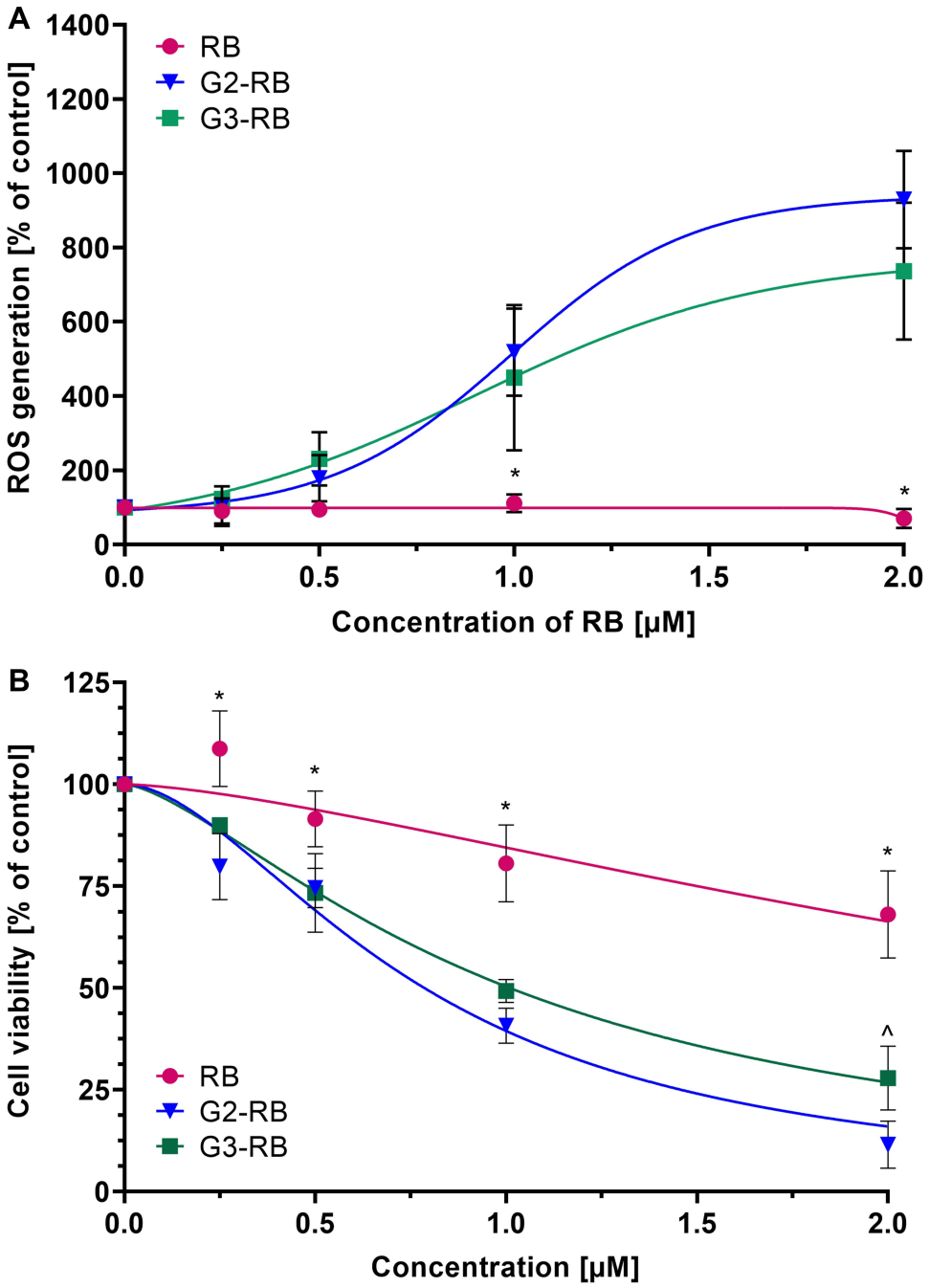

Figure 8 (**A**) ROS generation and (**B**) phototoxic activity of free RB and RB-loaded dendrimersomes (G2-RB and G3-RB) on AsZ cells. Data are presented as means ± SD, n=3. *Statistically significant difference at p<0.05 between RB and G2-RB or G3-RB. ^ Statistically significant difference at p<0.05 between G2-RB and G3-RB.

A promising approach for the design of therapeutic formulations is based on hyperbranched molecules - dendrimers and dendrons. Their advantages include monodisperse and reproducible molecular structure, combined with inherent multivalency.[37,38] Such a feature provides dendritic molecules with considerable activity at nano-bio interface, both as drug carriers and therapeutic entities themselves. Nanoformulations based on dendrimers and dendrons have been used to deliver low-molecular bioactive compounds,[39,40] therapeutic nucleic acids,[41,42] peptides and proteins[43] into target cells.

In particular, using amphiphilic dendrons as building blocks, it is possible to obtain supramolecular formulations with micellar or vesicular architecture.[21,44,45] The properties and morphology of dendritic assemblies depend on the size and topology of the dendron scaffold, the arrangement of chemical moieties within the dendron structure, and specifically selected hydrophilic and hydrophobic elements. Upon assembly, low-molecular weight drugs can be encapsulated either in the inner cavity or in the bilayer and can also be retained on the vesicle surface through complexation. Encapsulation protects a drug from degradation en route to the tumor.[22] Carbosilane dendritic architecture is versatile for designing functional systems for therapy,[46–49] imaging[50] and nanoparticle decoration.[51–53] Furthermore, the chemical structure of carbosilane dendrons containing two orthogonal functionalities favors the synthesis of amphiphilic derivatives self-organizing into micelles[54–56] or dendrimersomes.[20]

In this study, we examined the performance of triazine–carbosilane dendrimersomes as nanocarriers for RB in PDT. A previous study showed that due to the presence of protonatable triazine fragments inside the scaffold, dendrimersomes are pH-sensitive. Under slightly acidic conditions, reorganization of the vesicular structure occurs, as evidenced by the change in hydrodynamic diameter of dendrimersomes (Figure 3) and shrinkage of a hydrophobic bilayer observed in TEM images (Figure S8). This behavior can be exploited to achieve drug delivery directly into the tumor acidic environment.[20,57] In the first part of the reaserch, we studied the loading of RB into dendrimersomes of triazine–carbosilane dendrons of the second and third generation. We observed wavelength shifts of maximum absorbance or fluorescence of the RB–dendrimersome formulations in comparison to free RB. This finding indicates interaction between anionic RB and protonated dendrons, as described in the literature,[58,59] providing evidence for the formation of stable RB-dendrimersome formulations. Moreover, we observed visible changes in the absorbance and fluorescence intensity before and after dialysis used to purify RB-loaded dendrimersomes from the non-bound RB in solution. These changes could be used to determine the encapsulation efficiency and drug loading capacity (Table 1), as reported previously.[20] Zeta potential measurements revealed highly positive surface potential, which may be beneficial for cellular uptake.[60] Because these dendrimersomes formed at neutral pH, and the structure of dendrimersomes reorganizes at acidic conditions to enable drug release, we tested the release of RB from dendrimersomes of both generations at pH 5.5. Release was much slower for G3, which may explain why singlet oxygen generation was significantly higher for G3-RB. Because interactions with cationic polymers increase singlet oxygen production by RB, we believe the slower release is due to the fact that RB interacts with G3 more strongly than with G2 dendrimersomes.[61] The specific activities of different generations of dendrons/dendrimersomes require further study. However, for photodynamic therapy, PS does not need to be released from the carrier if the carrier allows diffusion of molecular oxygen.[4,62]

In an in vitro model using basal cell carcinoma cell lines, both flow cytometry and confocal microscopy revealed that cellular uptake of RB encapsulated in dendrimersomes was significantly greater than uptake of RB. This dramatic increase is likely due to the shielding of negatively charged groups in the RB structure by the positive surface charge of dendrimersomes. Nanoparticles with positive surface charges exhibit much more efficient intracellular transport. This phenomenon has been widely described in the literature and allows us to predict the behavior of nanosystems.[63–66] In the case of RB, increased cellular uptake seems to be critical for phototoxic activity: regardless of the level of singlet oxygen generation, RB-loaded dendrimersomes generate significantly higher levels of intracellular ROS, which translates into a stronger phototoxic effect. The IC_{50} values for RB-loaded dendrimersomes in vitro are remarkably low (~1 μM RB for both formulations), considerably lower than those for most formulations mentioned above (for instance[28,30,32,36]). Importantly, the dark toxicity of RB-loaded dendrimersomes is negligible in the concentration range used. It should be also noted that under the same conditions, empty dendrimersomes did not exert cytotoxic or phototoxic activity, so the observed results should not be attributed to additive or synergistic effects.

Conclusion

Our findings suggest that dendrimersomes built of amphiphilic triazine–carbosilane dendrons are robust vehicles for delivering RB into basal skin cancer cells, increasing the therapeutic performance of the PS through increased cellular uptake and intracellular ROS generation. This highly encouraging outcome sheds new light on PDT of skin cancers. However, further research is needed to answer the fundamental questions: how does RB interact with the carrier? How strong are these interactions? What is the localization of RB in the dendrimersome? What influences the difference in the

interactions of G2 and G3 with RB? Further studies on this system are also needed in term of intracellular localization of RB-loaded dendrimersomes and possibility of lysosomal escape, as well as in vivo activity.

Acknowledgments

The authors thank Dr. Julia Poletaeva and Prof. Elena Ryabchikova (ICBFM) for the TEM study of dendrimersomes and Dr. Ervin Epstein (Children's Oakland Research Institute, Oakland, CA, USA) for providing murine basal cell carcinoma lines (AsZ, BsZ, CsZ). This work was supported by National Science Centre, Poland (Project UMO-2017/25/B/NZ7/01304 "Phosphorus dendrimers as carriers for photosensitizers - in vivo studies"), by RFBR grant No. 18-33-20109, and based upon work from COST Action CA17140 NANO2CLINIC "Cancer Nanomedicine - from the bench to the bedside" supported by COST (European Cooperation in Science and Technology). The project received funding from the European Union's Horizon 2020 research and innovation programme under the Marie Skłodowska-Curie grant agreement No 844217. This work was also supported by PID2020-112924RB-I00 (Ministry of Science and Innovation), Consortium IMMUNOTHERCAN-CM B2017/BMD-3733 (CAM), NANODENDMED II-CM ref B2017/BMD-3703 and project SBPLY/17/180501/000358 JCCM and PIE14/00061 (CIBER-BBN).

Disclosure

The authors report no conflicts of interest in this work.

References

1. Basset-Seguin N, Herms F. Update on the management of basal cell carcinoma. *Acta Derm Venereol*. 2020;100(11):284–290. doi:10.2340/00015555-3495
2. Olivo M, Bhuvaneswari R, Lucky SS, Dendukuri N, Thong PSP. Targeted therapy of cancer using photodynamic therapy in combination with multi-faceted anti-tumor modalities. *Pharmaceuticals*. 2010;3(5):1507–1529. doi:10.3390/ph3051507
3. Kucinska M, Skupin-Mrugalska P, Szczolko W, et al. Phthalocyanine derivatives possessing 2-(morpholin-4-yl) ethoxy groups as potential agents for photodynamic therapy. *J Med Chem*. 2015;58(5):2240–2255. doi:10.1021/acs.jmedchem.5b00052
4. Sztandera K, Gorzkiewicz M, Klajnert-Maculewicz B. Nanocarriers in photodynamic therapy—in vitro and in vivo studies. *Wiley Interdiscip Rev Nanomed Nanobiotechnol*. 2020;12(3):1–24. doi:10.1002/wnan.1599
5. Pham TC, Nguyen VN, Choi Y, Lee S, Yoon J. Recent strategies to develop innovative photosensitizers for enhanced photodynamic therapy. *Chem Rev*. 2021;121(21):13454–13619. doi:10.1021/acs.chemrev.1c00381
6. Redmond RW, Gamlin JN. A compilation of singlet oxygen yields from biologically relevant molecules. *Photochem Photobiol*. 1999;70(4):391–475. doi:10.1111/j.1751-1097.1999.tb08240.x
7. Vanerio N, Stijnen M, De Mol BAJM, Kock LM. Biomedical applications of photo- and sono-activated rose bengal: a review. *Photobiomodulation Photomed Laser Surg*. 2019;37(7):383–394. doi:10.1089/photob.2018.4604
8. Demartis S, Obinu A, Gavini E, Giunchedi P, Rassu G. Nanotechnology-based rose Bengal: a broad-spectrum biomedical tool. *Dye Pigment*. 2021;188:109236. doi:10.1016/j.dyepig.2021.109236
9. Qidwai A, Annu NB. Role of nanocarriers in photodynamic therapy. *Photodiagnosis Photodyn Ther*. 2020;30:101782. doi:10.1016/j.pdpdt.2020.101782
10. Xie J, Wang Y, Choi W, et al. Overcoming barriers in photodynamic therapy harnessing nano-formulation strategies. *Chem Soc Rev*. 2021;50(16):9152–9201. doi:10.1039/d0cs01370f
11. Antimisiaris SG, Marazioti A, Kannavou M, et al. Overcoming barriers by local drug delivery with liposomes. *Adv Drug Deliv Rev*. 2021;174:53–86. doi:10.1016/j.addr.2021.01.019
12. Ghaffari M, Dehghan G, Baradaran B, et al. Co-delivery of curcumin and Bcl-2 siRNA by PAMAM dendrimers for enhancement of the therapeutic efficacy in HeLa cancer cells. *Colloids Surf B Biointerfaces*. 2020;188:110762. doi:10.1016/j.colsurfb.2019.110762
13. Duncan R, Izzo L. Dendrimer biocompatibility and toxicity. *Adv Drug Deliv Rev*. 2005;57(15):2215–2237. doi:10.1016/j.addr.2005.09.019
14. Tripathi PK, Tripathi S. Dendrimers for anticancer drug delivery. *Pharm Appl Dendrimers*. 2019;4:131–150.
15. Sztandera K, Gorzkiewicz M, Dias Martins AS, et al. Noncovalent interactions with PAMAM and PPI dendrimers promote the cellular uptake and photodynamic activity of rose bengal: the role of the dendrimer structure. *J Med Chem*. 2021;64(21):15758–15771. doi:10.1021/acs.jmedchem.1c01080
16. Zhou D, Fei Z, Jin L, et al. Dual-responsive polymersomes as anticancer drug carriers for the co-delivery of doxorubicin and paclitaxel. *J Mater Chem B*. 2021;9(3):801–808. doi:10.1039/D0TB02462G
17. Laskar P, Dufès C. Emergence of cationic polyamine dendrimersomes: design, stimuli sensitivity and potential biomedical applications. *Nanoscale Adv*. 2021;3(21):6007–6026. doi:10.1039/D1NA00536G
18. Laskar P, Somani S, Campbell SJ, et al. Camptothecin-based dendrimersomes for gene delivery and redox-responsive drug delivery to cancer cells. *Nanoscale*. 2019;11(42):20058–20071. doi:10.1039/C9NR07254C
19. Laskar P, Somani S, Altwaijry N, et al. Redox-sensitive, cholesterol-bearing PEGylated poly (propylene imine)-based dendrimersomes for drug and gene delivery to cancer cells. *Nanoscale*. 2018;10(48):22830–22847. doi:10.1039/C8NR08141G
20. Apartsin E, Knauer N, Arkhipova V, et al. pH-sensitive dendrimersomes of hybrid triazine-carbosilane dendritic amphiphiles-smart vehicles for drug delivery. *Nanomaterials*. 2020;10(10):1899. doi:10.3390/nano10101899

21. Percec V, Wilson DA, Leowanawat P, et al. Self-assembly of janus dendrimers into uniform dendrimersomes and other complex architectures. *Science (80-)*. 2010;328(5981):1009–1014. doi:10.1126/science.1185547
22. Hu FF, Sun YW, Zhu YL, Huang YN, Li ZW, Sun ZY. Enthalpy-driven self-assembly of amphiphilic Janus dendrimers into onion-like vesicles: a Janus particle model. *Nanoscale*. 2019;11(37):17350–17356. doi:10.1039/C9NR05885K
23. Estrella V, Chen T, Lloyd M, et al. Acidity generated by the tumor microenvironment drives local invasion. *Cancer Res*. 2013;73(5):1524–1535. doi:10.1158/0008-5472.CAN-12-2796
24. Fuentes-Paniagua E, Peña-González CE, Galán M, Gómez R, De La Mata FJ, Sánchez-Nieves J. Thiol-ene synthesis of cationic carbosilane dendrons: a new family of synthons. *Organometallics*. 2013;32(6):1789–1796. doi:10.1021/om301217g
25. Jones OT, Ranmuthu CKI, Hall PN, Funston G, Walter FM. Recognising skin cancer in primary care. *Adv Ther*. 2020;37(1):603–616. doi:10.1007/s12325-019-01130-1
26. Dabrzalska M, Janaszewska A, Zablocka M, Mignani S, Majoral JP, Klajnert-Maculewicz B. Complexing methylene blue with phosphorus dendrimers to increase photodynamic activity. *Molecules*. 2017;22(3). doi:10.3390/molecules22030345
27. Lutkus LV, Rickenbach SS, McCormick TM. Singlet oxygen quantum yields determined by oxygen consumption. *J Photochem Photobiol a Chem*. 2019;378:131–135. doi:10.1016/j.jphotochem.2019.04.029
28. Demartis S, Rassu G, Murgia S, Casula L, Giunchedi P, Gavini E. Improving dermal delivery of rose bengal by deformable lipid nanovesicles for topical treatment of melanoma. *Mol Pharm*. 2021;18(11):4046–4057. doi:10.1021/acs.molpharmaceut.1c00468
29. Ali MFM. Topical delivery and photodynamic evaluation of a multivesicular liposomal Rose Bengal. *Lasers Med Sci*. 2011;26(2):267–275. doi:10.1007/s10103-010-0859-9
30. Forouz F, Dabbaghi M, Namjoshi S, Mohammed Y, Roberts MS, Grice JE. Development of an oil-in-water self-emulsifying microemulsion for cutaneous delivery of rose Bengal: investigation of anti-melanoma properties. *Pharmaceutics*. 2020;12(10):1–17. doi:10.3390/pharmaceutics12100947
31. Torres-Martínez A, Bedrina B, Falomir E, et al. Non-polymeric nanogels as versatile nanocarriers: intracellular transport of the photosensitizers rose bengal and hypericin for photodynamic therapy. *ACS Appl Bio Mater*. 2021;4(4):3658–3669. doi:10.1021/acsabm.1c00139
32. Yeh HP, Del Valle AC, Syu MC, Qian Y, Chang YC, Huang YF. A new photosensitized oxidation-responsive nanoplatform for controlled drug release and photodynamic cancer therapy. *ACS Appl Mater Interfaces*. 2018;10(25):21160–21172. doi:10.1021/acsami.8b05205
33. Yan Y, Li J, Zheng J, et al. Poly (l-lysine)-based star-block copolymers as pH-responsive nanocarriers for anionic drugs. *Colloids Surf B Biointerfaces*. 2012;95:137–143. doi:10.1016/j.colsurfb.2012.02.034
34. Wang HY, Hou L, Li HL, et al. A nanosystem loaded with perfluorohexane and rose bengal coupled upconversion nanoparticles for multimodal imaging and synergetic chemo-photodynamic therapy of cancer. *Biomater Sci*. 2020;8(9):2488–2506. doi:10.1039/C9BM02081K
35. Han S, Hwang BW, Jeon EY, et al. Upconversion nanoparticles/hyaluronate-rose bengal conjugate complex for noninvasive photochemical tissue bonding. *ACS Nano*. 2017;11(10):9979–9988. doi:10.1021/acsnano.7b04153
36. Chen K, Chang C, Liu Z, et al. Hyaluronic acid targeted and pH-responsive nanocarriers based on hollow mesoporous silica nanoparticles for chemo-photodynamic combination therapy. *Colloids Surf B Biointerfaces*. 2020;194:111166. doi:10.1016/j.colsurfb.2020.111166
37. Mignani S, Rodrigues J, Roy R, et al. Exploration of biomedical dendrimer space based on in-vivo physicochemical parameters: key factor analysis (Part 2). *Drug Discov Today*. 2019;24(5):1184–1192. doi:10.1016/j.drudis.2019.03.001
38. Dias AP, da Silva Santos S, da Silva JV, et al. Dendrimers in the context of nanoMedicine. *Int J Pharm*. 2020;5:573.
39. Sandoval-Yañez C, Rodriguez CC. Dendrimers: amazing platforms for bioactive molecule delivery systems. *Materials*. 2020;13(3):570. doi:10.3390/ma13030570
40. Bolu BS, Sanyal R, Sanyal A. Drug delivery systems from self-assembly of dendron-polymer conjugates. *Molecules*. 2018;23(7):1570. doi:10.3390/molecules23071570
41. Mendes LP, Pan J, Torchilin VP. Dendrimers as nanocarriers for nucleic acid and drug delivery in cancer therapy. *Molecules*. 2017;22(9):1401. doi:10.3390/molecules22091401
42. Dzmitruk V, Apartsin E, Ihnatsyeu-Kachan A, Abashkin V, Shcharbin D, Bryszewska M. Dendrimers show promise for siRNA and microRNA therapeutics. *Pharmaceutics*. 2018;10(3):126. doi:10.3390/pharmaceutics10030126
43. Knauer N, Pashkina E, Apartsin E. Topological aspects of the design of nanocarriers for therapeutic peptides and proteins. *Pharmaceutics*. 2019;11(2):91. doi:10.3390/pharmaceutics11020091
44. Peterca M, Percec V, Leowanawat P, Bertin A. Predicting the size and properties of dendrimersomes from the lamellar structure of their amphiphilic janus dendrimers. *J Am Chem Soc*. 2011;133(50):20507–20520. doi:10.1021/ja208762u
45. Apartsin E, Caminade AM. Supramolecular self-associations of amphiphilic dendrons and their properties. *Chem – a Eur J*. 2021;27(72):17976–17998. doi:10.1002/chem.202102589
46. Fernandez J, Acosta G, Pulido D, et al. Carbosilane dendron-peptide nanoconjugates as antimicrobial agents. *Mol Pharm*. 2019;16(6):2661–2674. doi:10.1021/acs.molpharmaceut.9b00222
47. Sepúlveda-Crespo D, De La Mata FJ, Gómez R, Muñoz-Fernández MA. Sulfonate-ended carbosilane dendrimers with a flexible scaffold cause inactivation of HIV-1 virions and gp120 shedding. *Nanoscale*. 2018;10(19):8998–9011. doi:10.1039/C8NR01664J
48. Krasheninina OA, Apartsin EK, Fuentes E, et al. Complexes of pro-apoptotic siRNAs and carbosilane dendrimers: formation and effect on cancer cells. *Pharmaceutics*. 2019;11(1):25. doi:10.3390/pharmaceutics11010025
49. Sánchez-Milla M, Muñoz-Moreno L, Sánchez-Nieves J, et al. Anticancer activity of dendriplexes against advanced prostate cancer from protumoral peptides and cationic carbosilane dendrimers. *Biomacromolecules*. 2019;20(3):1224–1234. doi:10.1021/acs.biomac.8b01632
50. Carloni R, Del Olmo NS, Ortega P, et al. Exploring the interactions of ruthenium (II) carbosilane metallodendrimers and precursors with model cell membranes through a dual spin-label spin-probe technique using EPR. *Biomolecules*. 2019;9(10):540. doi:10.3390/biom9100540
51. Gutierrez-Ulloa CE, Buyanova MY, Apartsin EK, Venyaminova AG, de la Mata FJ, Gómez R. Carbon nanotubes decorated with cationic carbosilane dendrons and their hybrids with nucleic acids. *ChemNanoMat*. 2018;4(2):220–230. doi:10.1002/cnma.201700351
52. Pędziwiatr-Werbicka E, Gorzkiewicz M, Horodecka K, et al. Silver nanoparticles surface-modified with carbosilane dendrons as carriers of anticancer siRNA. *Int J Mol Sci*. 2020;21(13):1–17. doi:10.3390/ijms21134647
53. González-García E, Gutiérrez Ulloa CE, de la Mata FJ, Marina ML, García MC. Sulfonate-terminated carbosilane dendron-coated nanotubes: a greener point of view in protein sample preparation. *Anal Bioanal Chem*. 2017;409(22):5337–5348. doi:10.1007/s00216-017-0479-3

54. Gutierrez-Ulloa CE, Buyanova MY, Apartsin EK, et al. Amphiphilic carbosilane dendrons as a novel synthetic platform toward micelle formation. *Org Biomol Chem*. 2017;15(35):7352–7364. doi:10.1039/C7OB01331K
55. Mencia G, Lozano-Cruz T, Valiente M, de la Mata J, Cano J, Gómez R. New ionic carbosilane dendrons possessing fluorinated tails at different locations on the skeleton. *Molecules*. 2020;25(4):807. doi:10.3390/molecules25040807
56. Mencia G, Lozano-Cruz T, Valiente M, et al. Evaluation of pH-dependent amphiphilic carbosilane dendrons in micelle formation, drug loading and HIV-1 infection. *Org Biomol Chem*. 2020;18(47):9639–9652. doi:10.1039/D0OB01867H
57. Filippi M, Catanzaro V, Patrucco D, Botta M, Tei L, Terreno E. First in vivo MRI study on theranostic dendrimersomes. *J Control Release*. 2017;248:45–52. doi:10.1016/j.jconrel.2017.01.010
58. Haba Y, Harada A, Takagishi T, Kono K. Synthesis of biocompatible dendrimers with a peripheral network formed by linking of polymerizable groups. *Polymer*. 2005;46(6):1813–1820. doi:10.1016/j.polymer.2005.01.004
59. Dabrzalska M, Zablocka M, Mignani S, Majoral JP, Klajnert-Maculewicz B. Phosphorus dendrimers and photodynamic therapy. Spectroscopic studies on two dendrimer-photosensitizer complexes: cationic phosphorus dendrimer with rose bengal and anionic phosphorus dendrimer with methylene blue. *Int J Pharm*. 2015;492(1–2):266–274. doi:10.1016/j.ijpharm.2015.06.014
60. Fröhlich E. The role of surface charge in cellular uptake and cytotoxicity of medical nanoparticles. *Int J Nanomedicine*. 2012;7:5577–5591. doi:10.2147/IJN.S36111
61. Dabrzalska M, Janaszewska A, Zablocka M, Mignani S, Majoral JP, Klajnert-Maculewicz B. Cationic phosphorus dendrimer enhances photodynamic activity of rose bengal against basal cell carcinoma cell lines. *Mol Pharm*. 2017;14(5):1821–1830. doi:10.1021/acs.molpharmaceut.7b00108
62. Gorzkiewicz M, Klajnert-Maculewicz B. Chapter 10 in dendrimers for drug delivery. In: Sharma A, Keservan R, editors. *Dendrimers as Nanocarriers for Anticancer Drugs*. Apple Academic Press; 2018:327–374.
63. Honary S, Zahir F. Effect of zeta potential on the properties of nano-drug delivery systems - A review (Part 1 and 2). *Trop J Pharm Res*. 2013;12(2):255–264.
64. Gorzkiewicz M, Deriu MA, Studzian M, et al. Fludarabine-specific molecular interactions with maltose-modified poly (propyleneimine) dendrimer enable effective cell entry of the active drug form: comparison with clofarabine. *Biomacromolecules*. 2019;20(3):1429–1442. doi:10.1021/acs.biomac.9b00010
65. Fox LJ, Richardson RM, Briscoe WH. PAMAM dendrimer - cell membrane interactions. *Adv Colloid Interface Sci*. 2018;257:1–18. doi:10.1016/j.cis.2018.06.005
66. Hong S, Leroueil PR, Janus EK, et al. Interaction of polycationic polymers with supported lipid bilayers and cells: nanoscale hole formation and enhanced membrane permeability. *Bioconjug Chem*. 2006;17(3):728–734. doi:10.1021/bc060077y